REVISTA MATÉRIA V.30
ISSN 1517-7076 articles e20250513, 2025

Improving seismic performance of RC structures using AAC blocks and polyurethane binder

Hakan Koman[1], Abdullah Niğdelioğlu[1]

[1]Istanbul Aydın University, Department of Civil Engineering. Istanbul, Türkiye.
e-mail: hakankoman@aydin.edu.tr, abdullahnigdelioglu@aydin.edu.tr

ABSTRACT

This study aims to propose a novel infill wall system for RC moment-resisting frames, using 250 mm thick AAC blocks and polyurethane binders. Numerical validation with Abaqus and SAP2000 in single-story frames showed strong agreement with previous experimental and numerical studies. In single-story frames, the proposed AAC block infills with polyurethane binder increased the lateral load capacity by approximately 23% after yielding, compared to frames with traditional hollow brick infills. This value also indicates a 70% increase relative to the bare frame. In the pushover analysis of three-story models, the proposed system approximately increased lateral load capacity by 38% when compared with the structure without any infill, whereas a traditional hollow brick wall only increased capacity by 12%. The proposed wall significantly increased energy consumption and reduced plastic hinge damage when compared with bare and traditionally infilled frames. Stress analysis indicated potential infill cracking at maximum drift. Overall, the system demonstrates promising potential for enhancing seismic performance in RC structures.

Keywords: Abaqus; Sap2000; Pushover; Infill wall; AAC block; Polyurethane binder.

1. INTRODUCTION

Despite the improvements in structural engineering and earthquake engineering fields over the past decades, powerful earthquakes still continue to threaten human lives worldwide, especially in developing countries, where a problematic, non-ductile RC building stock still exists. In 2023, consecutive earthquakes measuring 7.8 and 7.6 in magnitude struck the Kahramanmaras region in Türkiye, causing a devastating catastrophe. In the region, during the earthquakes, PGA (peak ground acceleration) values around 0.8g were detected in the Antakya region [1]. In the Turkish Seismic Code (TSC 2018) [2], the highest level of earthquake is the DD1 level with a 2475-year return period and the design earthquake is the DD2 level with a 475-year return period. Due to the high PGA values, the corresponding peak spectral acceleration (PSA) values exceeded the ones determined for DD2 level. In particular, for short-period structures (0–0.5 s range), the PSA values exceeded the maximum considered earthquake spectrum associated with a 2475-year return period (DD1), as defined in the TSC 2018 [3]. When stronger ground motions than expected happen, energy dissipation, sufficient rigidity, and sufficient strength become vital to save lives.

Thus, previous researchers focused on strengthening of RC structures by improving energy dissipation and rigidity. The most conventional approach to seismic retrofitting is the addition of reinforced concrete (RC) shear walls. However, due to the complexities and challenges associated with the construction process, there is a growing demand for more practical and easily implementable solutions. Application of seismic dampers to moment frame structures is one of the practical methods. Three distinct metallic damper types were utilized in a previous study to enhance structural performance. In both steel and RC structures, dampers were positioned between the beams and the steel diagonal members. The MYFD (a hybrid damper combining metallic yielding and friction) exhibited the highest energy dissipation. According to the analysis results for the RC structure, the MYFD damper reduced its displacement response by around 35% [4]. In a different study [5], a 9-story RC structure was equipped with pall friction dampers. Given the rectangular shape of their hysteretic loops, dampers were represented using nonlinear link elements in the ETABS software model. Based on the dynamic analysis conducted using the El Centro 1940 earthquake record, in the analysis performed using pall friction dampers, the reductions in story displacements, column axial loads, shear forces, and bending moments were reported as 15.7%, 50.75%, 30.75%, and 27.24%, respectively [5].

Corresponding Author: Hakan Koman Received on 14/06/2025 Accepted on 02/10/2025

DOI: https://doi.org/10.1590/1517-7076-RMAT-2025-0513

Although seismic dampers are effective in seismic retrofitting process, they can cause the elimination of some of the infill walls inside the structure. While often overlooked for architectural reasons, infill walls play a critical role in structural behavior and must be accounted for in analysis. Infill walls are required to be included in both irregularity evaluation and structural modeling under Eurocode 8 [6], provided that they affect the lateral stiffness of the system. Despite addressing the significance of these elements, the code does not elaborate on detailed modeling procedures. FEMA-356, on the other hand, offers a clear formulation for modeling infill walls and recommends using either finite element analysis or the equivalent diagonal strut method to account for their effects. However, the method outlined in FEMA-356 for the equivalent strut approach does not consider the influence of vertical loading [6]. Similarly, TSC 2018 expresses that if there is no gap between the wall and the frame elements and a rigid connection is established, the structure needs to be designed with greater rigidity because the effective relative story drift limit is half of that in the case of a flexible connection [2].

On the other hand, transforming infill walls to energy-dissipating devices can be a practical solution. A study [7] was conducted to determine the damping ratio of frames incorporating mortarless masonry infill walls. A damping ratio of 0.03 was observed for the bare frame, while the addition of mortarless masonry infill increased the ratio to 0.17. Compared to the bare frame and the traditionally infilled frame, the structure utilizing mortarless walls shows a greater capacity for energy absorption [7]. In another study [8], experimental findings indicated that after axial load-induced column failure, mortarless semi-interlocking masonry blocks helped sustain axial loads and maintained energy dissipation via friction at block interfaces in the inelastic response phase. Compared to bare frames, those with semi-interlocking masonry infills exhibited significantly improved lateral load resistance, with an increase of approximately 1.4 times. Under lateral loading, the semi-interlocking brick masonry infill exhibited a fictitious diagonal compression strut mechanism, as noted by the researchers [8]. A comparative analysis was conducted in another study [9] on several types of pliable masonry infill equipped with horizontal sliding interfaces. Experimental hysteresis loops of infilled frames were first captured, and subsequently, numerical analyses were performed to simulate mortarless infill behavior through equivalent strut modeling. Subsequently, nonlinear incremental static analysis and nonlinear time history analysis were conducted on a six-story reinforced concrete structure, and findings indicated that incorporating a horizontally sliding joint within one type of flexible masonry infill resulted in a structural capacity increase by 1.6 times over the frame lacking any wall units [9]. Another research effort [10] explored diverse joint materials, showing that connecting the dry-stack wall rigidly to the steel frame enhanced energy absorption during lateral loading conditions, surpassing the performance of foam-jointed alternatives. This variation can be attributed to the greater vertical mobility allowed by the foam-filled joints in the infill when subjected to lateral forces. In contrast, the rigid connection increased friction between the mortarless blocks. Even if the infill walls consist of mortarless blocks sliding on top of each other, the type of joint between the wall and the RC frame will change the behavior [10].

For the design of RC structures in earthquake-prone regions, decreasing the weight of structures can be beneficial. For that purpose, in infill wall applications autoclaved aerated concrete blocks (AAC blocks) are used in practice. AAC material is a lightweight material due to its cellular structure, which contains air pockets. Although AAC blocks do not have high strength, in recent studies it's shown that strengthening of AAC masonry using fabric materials is possible. In a previous study [11], AAC masonry wallettes were strengthened using a fabric-reinforced cementitious matrix, and they were subjected to in-plane shear loading and out-of-plane loading. It was concluded that the increase in shear strength was around 1.7–1.8 times and the improvement in flexural capacity was around 4.7–6.9 times [11]. In another study [12], a detailed review for confined masonry walls strengthened with an externally bonded cementitious matrix was presented. Epoxy-based methods and cementitious-based techniques were investigated. It was concluded that in most of the specimens cementitious-based techniques were better for strength enhancement [12]. In another study [13], two externally bonded composites for masonry strengthening were investigated. Glass fabric–reinforced cement mortar (GF-RCM) and short-fiber engineered cementitious composite (SF-ECC) were used. Laboratory tests showed that both methods improved tensile and bond performance, with SF-ECC achieving higher strengths, while GF-RCM offered better practical applicability for field retrofitting [13]. Also, sometimes the windows and door openings can be critical zones in a masonry wall; thus, another study [14] investigated externally bonded composites for improving the seismic performance of confined masonry (CM) walls with openings. Fabric-reinforced cementitious matrix bands and hybrid short-fiber cementitious composites were applied to CM walls with window and door openings. The strengthened walls showed notable enhancements, with in-plane capacity rising 1.7 times and energy dissipation increasing 3.7 times [14].

In that investigation, the idea of transforming infill walls to energy dissipating systems is still supported; however, some modifications were proposed. It's considered to create a novel infill configuration designed to improve the frame's lateral stiffness and energy dissipation and simultaneously support internal vertical load

transfer. For that purpose, instead of mortar, a polyurethane-based binder with high deformation capacity was used. A prior study [15] employed this injection material within the interaction region between conventional hollow brick infill and the reinforced concrete frame. It was observed during the in-plane shear evaluation that the use of polymer injection led to increased ductility in the tested frame assemblies [15]. In a different experimental study, dynamic loading tests demonstrated that the injected polymer prevented the collapse of the interaction region and protected the hollow block infill up to a 2.5% drift level [16]. AAC blocks were identified as the primary component of the infill wall. The proposed infill wall eliminates the disadvantages of mortarless masonry, which was proposed previously, because polyurethane binder strengthens the infill against failure in the out-of-plane direction, and its high deformation capacity and flexibility provide energy dissipation and lower stresses between blocks. For mortarless masonry, generally solid clay blocks or concrete blocks were applied despite the fact that block strength does not contribute to the frame's lateral strength very significantly. Furthermore, using concrete blocks/solid clay blocks will increase the total weight of structures. AAC blocks are advantageous for decreasing the weight of structures, increasing the insulation, and the polyurethane binder still provides energy dissipation. To analyze the proposed infill wall, first, a FEM (finite element method) analysis was performed by Abaqus in single-story RC frames, and the effect of the proposed wall on the behavior was understood. Later, the analysis was improved using SAP2000 software, which allows a more practical approach in modeling. Finally, an incremental nonlinear static analysis (pushover) was performed on 3-story structures.

2. NUMERICAL MODELLING

2.1. Reinforced concrete frame model

Reinforced concrete frames used in this study were based on previous works incorporating experimental tests alongside finite element analysis carried out with Abaqus software [17, 18]. This selection of frames facilitates a direct evaluation of the outcomes presented in this study against prior findings derived from both experimental testing and numerical modeling. Nevertheless, the steel and concrete materials were substituted with regionally equivalent materials commonly used in Europe. ZHAI *et al.* [17] utilized a concrete compressive strength of 27.74 MPa in their Abaqus simulation, in contrast to the 30 MPa value used in the subsequent study by KOMAN [18]. In Abaqus simulations, the compressive strength of concrete is typically defined based on cube test values. The reinforcement properties varied between studies; for longitudinal rebars, ZHAI *et al.* [17] used steel with 472 MPa yield and 656 MPa tensile strength, while KOMAN [18] applied longitudinal rebars with 491 MPa yield and 553 MPa tensile capacity. In terms of confinement reinforcement, ZHAI *et al.* [17] used steel rated at 308 MPa for yield strength, whereas KOMAN [18] adopted 277 MPa. In that study, the material properties of the frame were assumed to be the same as in a past study [18].

Three different reinforced concrete frame models were analyzed under quasi-static loading conditions using the Abaqus software. One frame contains no infill wall, the second frame contains a hollow brick infill wall, which is widely used in the construction sector, and the third frame contains the proposed energy-dissipating wall system, which is composed of AAC blocks and a polyurethane binder.

The geometric specifications of the RC frame and the reinforcement details are available in previous research [17, 18]. Each column had a height of 3000 mm in the modeled frame. The length of the bay from the inner side of one column to the other column's inner side was 2800 mm. The columns had a square cross-section of 350 mm by 350 mm, whereas the beams featured a rectangular cross-section measuring 350 mm by 400 mm. Longitudinal reinforcement in the columns consisted of 8ϕ16 bars, while 4ϕ16 bars were used in the beams. Stirrups with a diameter of 8 mm were placed with 100 mm of spacing in critical regions and 150 mm in non-critical zones for both beams and columns as confinement reinforcement. In the computational model, fixed boundary conditions were assigned to the column bases. An axial force of 700 kN (the column was subjected to a surface load of 5.71 MPa to represent axial force conditions) was introduced as vertical loading. The frame properties are illustrated in Figure 1, which was recreated based on the previous studies [17, 18].

2.2. Modeling of concrete and steel in abaqus

Concrete behavior was modeled using the CDP (Concrete Damaged Plasticity) approach implemented within the Abaqus software. The Concrete Damaged Plasticity model is a constitutive framework utilized to simulate the plastic deformation behavior of materials subjected to various stress conditions. To analyze material response under loading, the stress tensor may be split into hydrostatic and deviatoric portions, corresponding to volumetric and distortion-related stresses, respectively. The Von Mises yield criterion suggests that hydrostatic stress may lead to reversible volumetric changes but does not contribute to plastic deformation. The permanent deformation is caused by the deviatoric stress tensor. Therefore, only the stresses responsible for deformation should be considered. According to the theory, the onset of plastic deformation is governed by the second

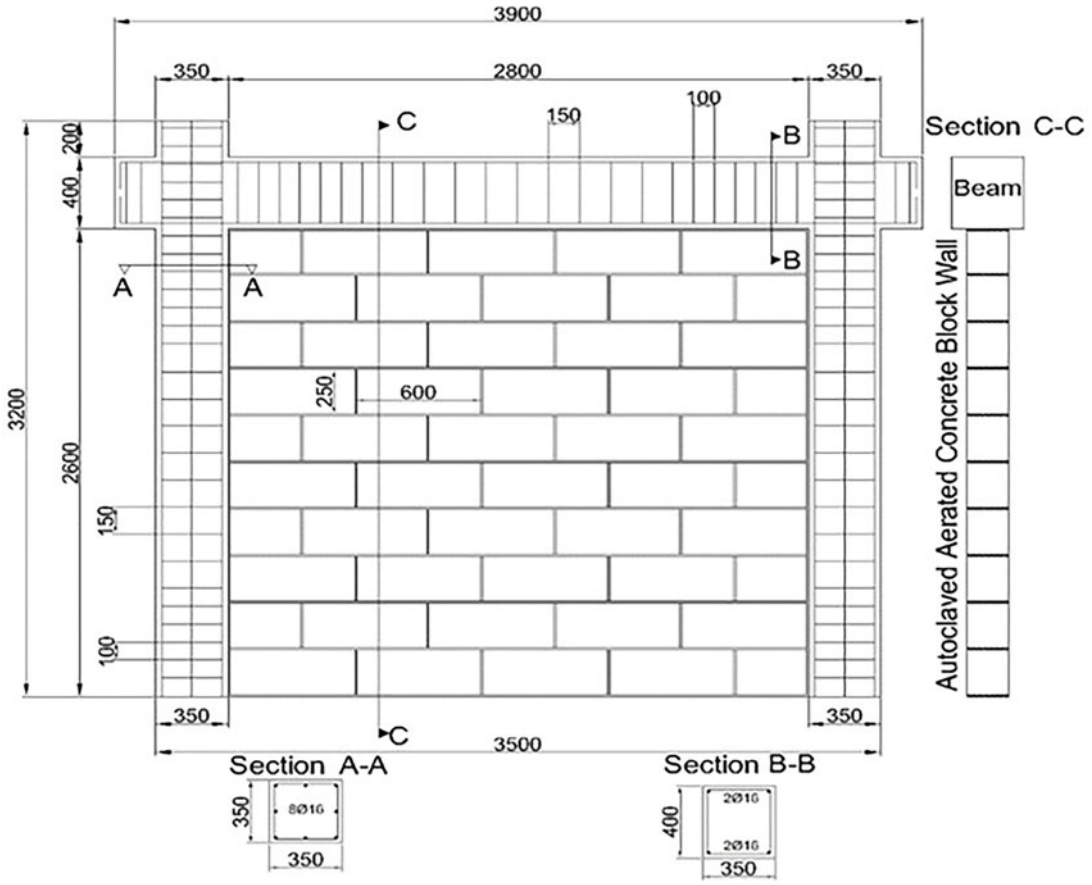

Figure 1: Structural layout of the RC frame with the integration of AAC masonry.

invariant of deviatoric stress (J2), which must exceed a certain critical value. The Drucker–Prager criterion accounts for hydrostatic pressure effects in combination with deviatoric stress, allowing it to represent both volumetric changes and plastic deformation behavior; features not captured by pressure independent models such as the Von Mises yield criterion.

The Concrete Damaged Plasticity (CDP) model is a modified form of the Drucker-Prager criterion. In the CDP model, the surface that defines yielding is adjusted using a K coefficient. In this manner, as shown in Figure 2, the conical yield surface varies [19]. The yield surface in Figure 2 is the yield surface of the CDP model when K = 2/3.

Abaqus utilizes the approach illustrated in Figure 3 [20] to determine the compressive stress–plastic strain relationship for concrete, ensuring an accurate representation of its nonlinear behavior under compressive loading. In Figure 3, the d_c coefficient characterizes the reduction in the elastic stiffness of concrete under compressive loading, reflecting the material's progressive damage and stiffness degradation behavior. In the modeling process, the d_c coefficient was assumed to be zero. The stress and strain values were determined using Equation 1, as described in the previous study [21]. The strain at maximum compressive strength (ε_0) for C25 grade concrete was taken as 0.0022 and the corresponding elastic modulus was assumed to be 31.000 MPa. In the analysis, the cube strength (f_0) of C25 grade concrete was taken as 30 MPa and this value must be entered into Abaqus. The Equation 1 [21] for determining the stress and strain values of concrete can be seen as follows:

$$\frac{f}{f_0} = 2.1\left(\frac{\varepsilon}{\varepsilon_0}\right) - 1.33\left(\frac{\varepsilon}{\varepsilon_0}\right)^2 + 0.2\left(\frac{\varepsilon}{\varepsilon_0}\right)^3 \quad (1)$$

The stress-strain relationships of concrete can be seen in Figure 4.

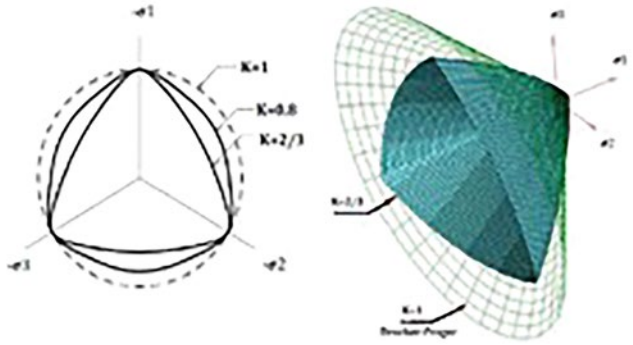

Figure 2: The yield surfaces of CDP model and drucker prager model [19].

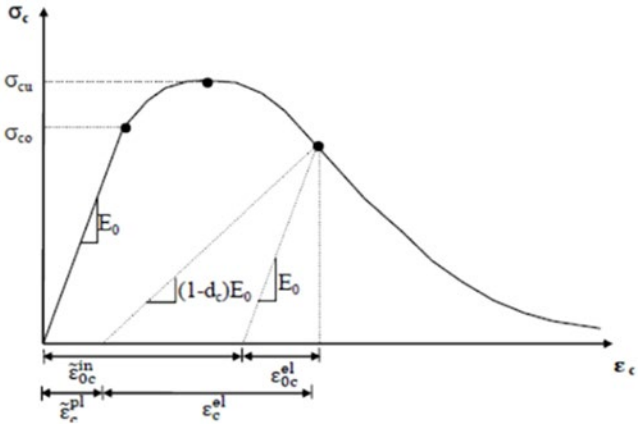

Figure 3: Modeling the stress–strain behavior of concrete in Abaqus [20].

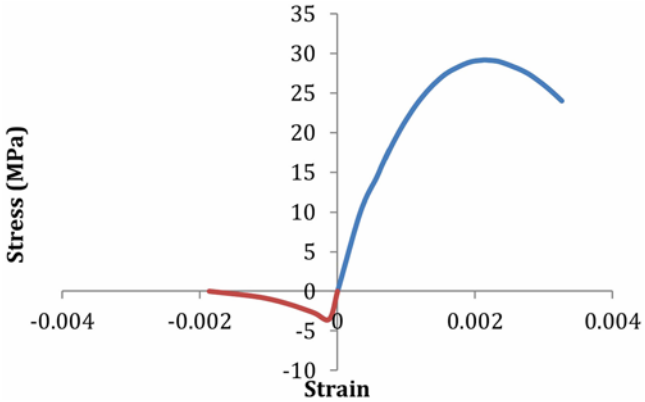

Figure 4: Stress–strain graph of concrete in Abaqus.

The tensile stress–strain behavior was considered linear up to the point of tensile strength, which was approximated as 0.7 multiplied by the square root of the characteristic compressive strength. An exponential softening response was defined beyond the tensile strength limit in the stress–strain relationship. The model included the effects of plastic deformation, and consistent with the approach used for compressive stress–strain behavior, the d_t parameter—representing the reduction in tensile stiffness of concrete—was assumed to be zero.

The implementation of the CDP model in Abaqus required the specification of several supplementary parameters. The dilation angle, indicating expansion in the p–q plane, eccentricity, defined as the ratio of concrete's tensile to compressive strength, and the f_{bo}/f_{co} ratio, which compares compressive strength under biaxial and uniaxial loading, were assigned values of 38°, 0.1, and 1.16, respectively. The values were derived from a previous experimental and numerical study [20], where the numerical outcomes exhibited significant concordance with the experimental results.

Two varieties of steel were examined in this study for longitudinal and confining rebars. The identical materials utilized in the previous study were employed [18]. The steel employed for longitudinal reinforcement exhibited a yield stress of 491 MPa and an ultimate tensile stress of 553 MPa. SAE-grade steel was used for the transverse reinforcement (stirrups), with a yield stress of 277 MPa and a maximum stress capacity of 387 MPa before failure. The analysis considers steel exhibiting identical mechanical behavior under both tensile and compressive loading conditions. In Abaqus, it is necessary to explicitly define the stress–strain relationships for the materials used in the analysis. A previous study [20] employed an elastic–perfectly plastic stress–strain model for steel in Abaqus, which produced simulation results that closely aligned with experimental observations. In a previous study [18], steel's behavior was modeled based on the approach of the TSC 2018 [2]. In this study, the approach of TSC 2018 was adopted. The stress-strain relations of steel are shown in Figure 5.

2.3. Modeling of polyurethane binder in abaqus

The polyurethane binder in this study was intended to be a polyurethane injection material in the sector. It consisted of two components that, when mixed, rapidly harden into a rubber-like substance. Rubber's stress-strain curve is different than metals. After the yielding plateau, an increase happens in strength in large deformations. Figure 6 [22] displays a typical stress-strain curve of hyperelastic materials. Hyperelastic materials,

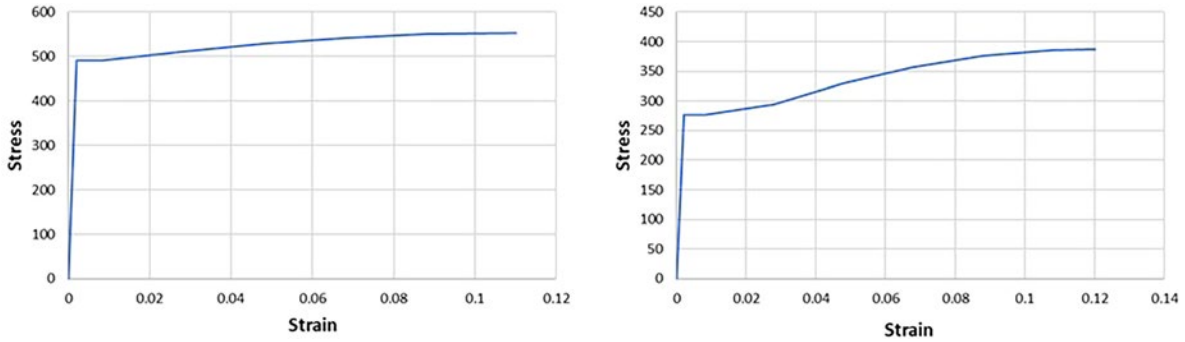

Figure 5: Stress-strain behaviour of steel materials [18].

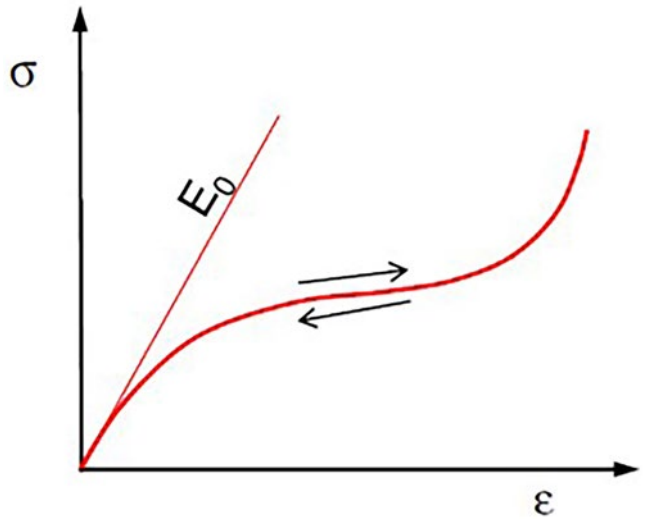

Figure 6: Stress-strain behaviour of hyperelastic materials [22].

such as rubber, can be represented by a strain energy function, which characterizes the area enclosed by the stress–strain curve.

Multiple hyperelastic models proposed in previous studies are based upon the strain energy formulation. In earlier research by KWIECIEN [23], the hyperelastic behavior of polyurethane binder placed between CFRP and masonry bricks was simulated based on the Mooney-Rivlin model. The Mooney-Rivlin model can be expressed by the following equations [23]:

$$W^{M\text{-}R} = C_{10} \times (\Delta^2 + 2/\Delta - 3) + C_{01} \times (1/\Delta^2 + 2\Delta - 3) \tag{2}$$

$$S_1 = F/A_0 = (\mathrm{d}W^{M\text{-}R}/\mathrm{d}\Delta) = 2 \times (C_{10} \times (\Delta - 1/\Delta^2) + (C_{01} \times (1 - 1/\Delta^3) = 2 \times (1 - 1/\Delta^3) \times (\Delta C_{10} + C_{01}) \tag{3}$$

$$E_0 = 3G_0 = 6\,(C_{10} + C_{01}) \tag{4}$$

$$G_0 = 2\,(C_{10} + C_{01}) \tag{5}$$

In equations, $W^{M\text{-}R}$ is the strain energy density function, S_1 is stress, F is force, A_0 is the initial cross-sectional area of the specimen, E_0 is the modulus of elasticity, G_0 is the shear modulus, and Δ is the ratio of final length to initial length. Tests are required to determine the coefficients in the equations. In this study a polyurethane injection material called polymer PM was applied. The tensile strength of polymer PM was 1.4 MPa at 140% strain level and its modulus of elasticity was 4 MPa, according to a previous study [24]. According to a more detailed experimental study [25], the compressive strength of polymer material was 12 MPa at 80% strain level. Also in that study [25], the coefficients of the Mooney-Rivlin theory were determined experimentally. The Mooney-Rivlin coefficients were taken as follows: $C_{01} = -0.05$ and $C_{10} = 0.47$. Further details can be found in the referenced studies [23, 24, 25].

2.4. Numerical modeling of the interface behavior between binder and masonry blocks in abaqus

Abaqus allows for the modeling of binder-material interaction through surface-based cohesive behavior, which effectively captures interface debonding and failure. In a previous study [26], the interaction between masonry walls and reinforced concrete tie-columns in confined masonry (CM) structures was investigated. Results indicated that surface-based cohesive behavior produced results closer to experimental data, capturing realistic opening, sliding, and progressive damage at the interface, whereas tie constraints overestimated stiffness and strength due to their rigid connection assumption. The traction–separation model enables accurate representation of connections characterized by negligible interface thickness, such as adhesive joints or thin bonding layers. Since the interface thickness between blocks was 1 cm, surface-based cohesive behavior was applied. In surface-based cohesive behavior modeling, joints under tensile and shear failure modes are characterized. Figure 7 provides an illustration of the traction-separation concept. At the initial stage of loading, the joint exhibits linear elastic behavior, with K_n, K_s, and K_t representing its stiffness. Following the attainment of peak interface traction, the bond begins to exhibit inelastic behavior. As shown in Figure 7, the maximum stress

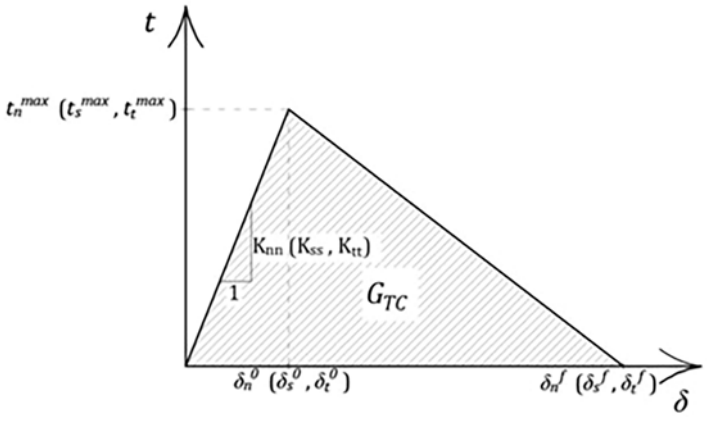

Figure 7: Traction-separation behavior [27].

values are t_n^{max}, t_s^{max}, t_t^{max}, while the separation values corresponding to these stresses are d_n^0, d_s^0, d_t^0, respectively. The separation values at failure are given as d_n^f, d_s^f, d_t^f [27].

Damage initiation was determined based on the maximum nominal stress criterion implemented within Abaqus. In the joints where mortar existed, the K_n value was 0.1N/mm^3, K_s and K_t were 0.337 N/mm^3. In the joints where polyurethane binder existed, the K_n value was 0.33N/mm^3, K_s and K_t were 0.088 N/mm^3. These values were adopted from previous studies [28, 29]. A Mohr-Coulomb frictional sliding model with a friction coefficient of 0.66 was utilized to represent the interface behavior after joint failure. Accordingly, the joint begins to slide once the applied shear stress goes beyond the prescribed failure limit. Defining friction after traction-separation laws was also used in a previous study [26] to simulate the interaction between masonry walls and reinforced concrete tie-columns in confined masonry (CM) structures. Fracture energies associated with the joints were derived from a previously conducted experimental study by VISKOVIC *et al.* [29]. In the previous study [29], experimental tests were carried out to determine the fracture energy values of the joints. Experimental results indicated that the modified fracture energy for flexible polymer PM joints reached 4.22 N/mm under tensile failure (Mode I) and 10.93 N/mm under shear failure (Mode II). These experimentally derived values were incorporated into the numerical model to simulate joint failure under tensile and shear conditions. To account for mixed-mode behavior, the Benzeggagh-Kenane rule was applied in Abaqus. According to ABDULLA *et al.* [27], the Benzeggagh-Kenane model is the most appropriate for capturing mixed-mode fracture behavior when the critical energies for Mode II and Mode III are equal, with an exponent of 2 typically used for brittle materials.

The study employed a mortar mix consisting of cement, lime, and sand in a 1:2:9 proportion, achieving a compressive strength of 5 MPa, consistent with the formulation used in prior investigations [18, 28]. In the referenced study, for joints incorporating mortar binders, the fracture energy was assumed to be 0.10 N/mm in Mode I (tension) and 0.183 N/mm in Mode II (shear). The CDP model for mortar adopted a dilation angle of 36.4°, with mechanical properties derived from experimental data [28]: compressive strength of 5 MPa, modulus of elasticity of 700 MPa, Poisson's ratio of 0.157, and tensile strength of 0.257 MPa.

2.5. Numerical modeling of masonry infill walls using abaqus

For the modeling of masonry, commonly three different approaches are used in literature. These are the micro-modelling approach, the simplified micro-modelling approach, and the macro-modelling approach. In the micro-modelling approach, the blocks, binder, and the interaction between blocks and binder are modelled separately. In the simplified micro-modeling approach, half of the binder and block are homogenized and the number of interacted surfaces decreases. In the macro-modeling approach, all of the assembly is assumed to be a homogenous material. In that study, in the modelling of AAC block wall micro-modeling approach was used. A macro-scale modeling approach was adopted for the traditional infill wall system constructed with hollow clay bricks and mortar. In a previous study [28], a comparison was performed using Abaqus software for hollow brick-infilled RC frames, and there was a small discrepancy between the load-displacement curves of the macro-modeled frame and the micro-modeled frame.

The AAC blocks were modeled again using the CDP model. The mechanical properties of blocks were taken from a previous study [30], which reported experimental results of AAC block specimens. According to the average values of stronger AAC specimens in a previous study [30], the compressive and flexural tensile strengths were adopted as 5 MPa and 1.44 MPa, respectively. The analysis considered an elastic modulus value of 2354 MPa. According to earlier research [30], the stress-strain curves of AAC block in compression and tension were determined to be nearly linear-elastic until maximum load and after the max. load, a very brittle failure occurred. That is why in that study, the behavior was assumed to be linear until the maximum load.

The wall modeling from the previous studies [18, 28] was adopted in this research. Hollow brick's and mortar's compressive strengths were taken as 3.56 MPa and 5 MPa, respectively, based on a previous experimental study [28]. The tensile strengths of hollow brick and mortar were taken as 0.9 MPa and 0.257 MPa, respectively. The modulus of elasticity of the homogenized wall was calculated using equation 10, as explained in section 2.7. The modulus of elasticity of hollow brick and mortar was taken as 1111 MPa and 700 MPa based on a previous study [28]. Based on equation 10, the modulus of elasticity of the homogenized wall was calculated as 1012.24 MPa. Within the macro-modeling framework, the mechanical properties of the infill wall, including compressive and tensile strengths, were estimated based on Eurocode-based formulations:

$$f_{ck} = 0.4 \times 3.56^{0.75} \times 5^{0.25} = 1.57\text{Mpa} \tag{6}$$

$$f_{ctk} = 0.4 \times 0.9^{0.75} \times 0.257^{0.25} = 0.26\text{Mpa} \tag{7}$$

In equations 6–7, f_{ck} is the nominal compressive strength of the homogenized wall, and f_{ctk} is the characteristic tensile strength. 0.75 and 0.25 indicate the percentage of volume of blocks and mortar. The corresponding tensile and compressive strengths of materials were used. Figure 8 displays the stress-strain relationships for the homogenized wall. These stress-strain values were adopted from a previous study [31]. In another study, for lime mortars, this type of linear idealization was applied for post-peak behavior [26].

The modeling of the homogenized masonry wall was also carried out using concrete damaged plasticity inside Abaqus. This approach was previously applied in the finite element analysis of confined masonry walls strengthened with a fabric-reinforced cementitious matrix [32].

2.6. Analysis details in abaqus

All materials, except for the reinforcing bars, were modeled using C3D8R elements, which are three-dimensional, eight-noded elements with reduced integration. The element sizes were set at 50 mm for the frame and wall and 10 mm for the binder material. In the simulation, rebars were represented by wire elements, ideal for modeling long and slender components embedded in solid structures. The B31 element, which is a 2-node beam element, was adopted for rebars. The mesh dimension for rebar elements was 125 mm. The reinforcement was fully bonded to the concrete domain using embedded region constraints to simulate composite behavior. Figure 9 illustrates the mesh configuration of the RC frame with AAC blocks and polyurethane binder. The frame was modeled with fixed supports at the base.

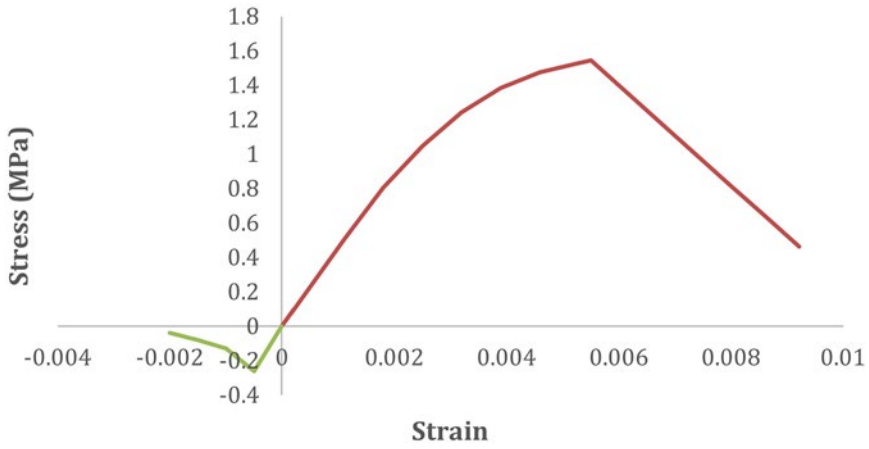

Figure 8: Stress-strain relationships of homogenized wall.

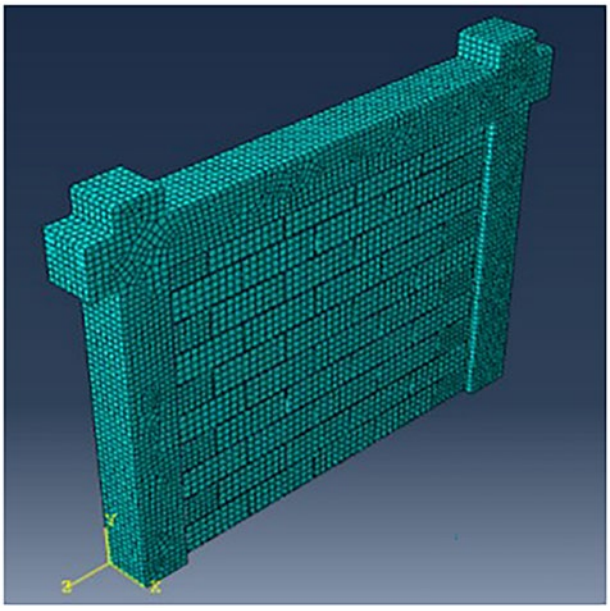

Figure 9: Finite elements of RC frame and AAC block.

An explicit dynamic analysis was conducted, in which the frame was subjected to lateral cyclic displacement loading reaching ±80 mm over a total duration of 31.97 seconds. During the hysteretic cycle, a constant pressure of 5.71 MPa was applied to columns. The finite element formulation in Abaqus begins with the computation of the system's stiffness, mass, and damping matrices. The central difference approach is utilized in explicit analysis to numerically solve the equation of motion. This method eliminates the need to reconstruct the stiffness, mass, and damping matrices at each time step by computing the displacement at step I+1 based on the values from steps I and I−1 [33].

Explicit dynamic analysis in Abaqus is considered computationally efficient, making it suitable for problems where minimal processing power is desired. In explicit dynamic analysis of quasi-static problems, maintaining low inertial effects is crucial to preserve the quasi-static nature of the simulation. This condition can be verified by monitoring the ratio of kinetic energy to total internal energy after the analysis. If this ratio remains below 0.10, the simulation is considered quasi-static [33].

2.7. Modeling of single-story frames in SAP2000 software

The reinforced concrete frame was modeled using beam elements in SAP2000, a software based on the finite element method. Subsequently, the non-linear incremental static loading procedure (pushover analysis) was applied to three different RC frame systems. In RC frames, the nonlinear behavior occurred mostly in column and beam ends; thus, plastic hinges were formed in these zones. In SAP2000, plastic hinges can be modeled at the end zones of elements. To achieve this, moment–curvature relationships of the RC sections were utilized and the interaction between axial load and flexural capacity in the columns was also considered. Plastic hinges were assumed to form at locations corresponding to 10% and 90% of the member length from each end. The hinge length was assumed to be 10% of the total member length.

Among the approaches presented in the literature for modeling infill walls, the equivalent diagonal strut method is widely adopted, as mentioned in the introduction. Link elements are commonly used in SAP2000 to simulate the behavior of equivalent diagonal struts representing infill walls. The method explained in previous studies [34, 35] was used in modeling of the link element. Link elements were modeled as multi-linear plastic link elements. For both the hollow brick infill wall frame and the AAC block frame with polyurethane binder, equivalent compressive struts were modeled using link elements. In equivalent compressive struts, the link behavior was modeled as a hysteretic pivot. For the wall with AAC blocks and polyurethane binder, the tensile resistance of polyurethane material was not neglected and the links that are subjected to tension were modeled using hysteretic isotropic behavior. The equations used in the creation of hysteretic pivot links are presented below [34, 35].

$$\lambda_1 = \sqrt[4]{\frac{E_{winf} t_{winf} sin(2.\theta)}{4.E_{cm} I_c h_{winf}}} \tag{8}$$

$$b_{winf} = \frac{0{,}175 r_{winf}}{(\lambda_1 . l_c)^{0,4}} \tag{9}$$

In equation 8, E_{winf} denotes the elastic modulus of the infill wall, t_{winf} denotes the thickness of the equivalent strut and the infill wall, θ indicates the aspect ratio, E_{cm} is the modulus of elasticity of the material used in the frame system, I_c refers to the moment of inertia of the columns, and h_{winf} is the height of the infill panel. In equation 9, r_{winf} represents the diagonal length (3770 mm) of the infill wall panel, and l_c denotes the height of the columns (2800 mm) between the centerlines of the beams.

In the frames, θ was equal to 43.60 degrees. In traditional hollow brick masonry, the modulus of elasticity was adopted as 1012 MPa based on a previous study [18]. For the wall constructed with AAC blocks and polyurethane binder, the modulus of elasticity was calculated using Equation 10 [36] as follows:

$$E_{wall} = \frac{(tt + th)}{\frac{tt}{Et} + \frac{th}{Eh}} \tag{10}$$

The total displacement of the masonry under load is the sum of the displacement of the mortar and the displacement of the brick. Applying Hooke's law and simplifying the calculations, Equation (10) was obtained.

In this equation, tt is the thickness of bricks, th is the thickness of binder, Et is the modulus of elasticity of brick material, Eh is the modulus of elasticity of binder material. The AAC block used in this study had a modulus of elasticity value of 2354 MPa; the polyurethane material had a modulus of elasticity value of 4.5 MPa. The binder thickness inside the wall was 10 mm. Thus, the modulus of elasticity of the wall was considered as 111.66 MPa. For the compression strut of both the traditional infill wall and the polyurethane infill wall, the multilinear compression strut type was selected as "Pivot". In the traditional infill wall model, only the compression strut was considered. The parameters and values used in the compression link for the traditional infill wall and AAC block wall are presented in Table 1 and Table 2. The points S_1, S_2, and S_3 on the compression envelope correspond to the yielding, peak, and restoring forces, respectively. δ_1, δ_2, and δ_3 correspond to the deformations at yielding (S1), peak strength (S2), and residual strength (S3), respectively (Figure 10).

Experimental results demonstrate that AAC Blocks and polyurethane binder model resists tension. For this reason, a tension link was incorporated into the polyurethane model. This link was considered relatively simple and therefore defined as kinematic. The parameters used for the tension strut are also presented in Table 3.

2.8. Modeling of multi-story buildings in SAP2000 software

In addition, after the analyses were performed on the single-story, one-bay frames, the models were compared in a 3-story reinforced concrete building in SAP2000 with nonlinear static pushover analysis. The multi-story structure featured a square plan with dimensions of 21 m × 21 m. In the structure the span length between columns was assumed to be 7 m. Each story was assumed to have a height of 3 meters. The assumed structure was a moment frame building which contains RC slabs. The structure was modeled using C25/30 concrete and S420 grade reinforcing steel. The structure was taken as representative of the Istanbul region, where a peak ground acceleration of around 0.4 g is typically expected. The parameters and materials used in the multi-story structure were summarized in Table 4. The structural system employed frame elements for columns and beams, thin shell elements for slabs and link elements to represent infill walls. Nonlinear behavior at the ends of beams

Table 1: Hollow brick infill wall – compression link.

S_1 (kN)	S_2 (kN)	S_3 (kN)	δ_1 (mm)	δ_2 (mm)	δ_3 (mm)
–35.437	–47.25	–9.45	–1.409	–4.504	–85.01

Table 2: AAC blocks and polyurethane binder – compression link.

S_1 (kN)	S_2 (kN)	S_3 (kN)	δ_1 (mm)	δ_2 (mm)	δ_3 (mm)
–158.51	–211.35	–42.37	–45.84	–809.87	–850.11

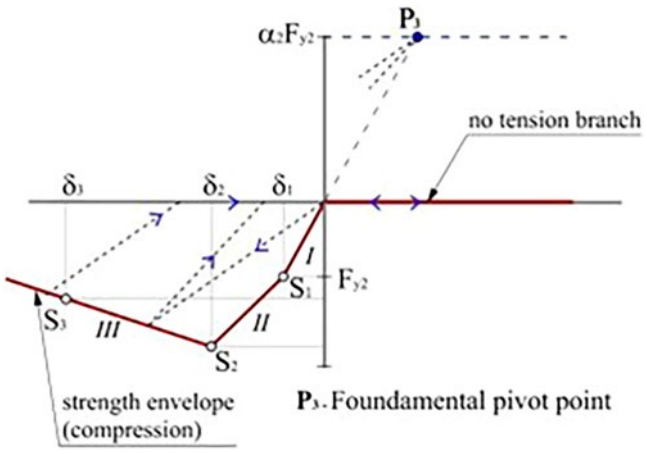

Figure 10: Specification of the hysteretic pivot law for the equivalent compressive diagonal strut [34].

Table 3: AAC Blocks and polyurethane binder – tension link.

DISPLACEMENT (mm)	FORCE (kN)
0	0
1	1.44

Table 4: Parameters used in multi-story building.

PARAMETER	PROPERTY
Concrete	C25/30
Rebar	S420
Column Dimension	40 cm × 40 cm
Beam Dimension	25 cm × 45 cm
Slab Thickness	15 cm
Column Rebar	8φ20
Beam Rebar Top	4φ12
Beam Rebar Bottom	4φ16
Distance between stir-ups	10 cm
Story Height	3 m

was modeled with M3 moment hinges, whereas in the end zones of columns, axial-moment interaction hinges (P-M2-M3 type) were used. To assign M3 hinges, only the moment-curvature relationship of the RC beam cross section was defined using the section designer inside SAP2000 and to define P-M2-M3 hinges also, the axial force-moment interaction surface of the RC column cross section was defined in the software. Based on TS498-1997, a 2 kN/m^2 live load and a 2.04 kN/m^2 floor covering dead load were assigned to the slabs. In the model with a hollow brick wall, 10 kN/m was assigned as a uniform wall load to the beams (a typical loading for a 20 cm wall with plaster), and a 5 kN/m (a typical loading for a 20 cm AAC block wall with plaster) uniform load was assigned to the beams in the model with a polyurethane binder. Before performing a lateral nonlinear static loading to the structure, a nonlinear vertical loading was applied to consider the decrease in the rigidity of cracked cross sections. This approach was adopted in TSC-2018 by considering the G+0.3Q load combination as the weight of the structure (for residential buildings) [2]. Here G indicates dead loads, and Q indicates live loads.

Three different models were created in SAP2000 software. The first model included no infill wall, the second model included an infill wall with hollow bricks, and the third model included infill walls with AAC blocks and polyurethane binders. In the middle bay, no walls were considered. A detailed plan of the multi-story structural frames, including infill walls, is provided in Figure 11.

3. RESULTS AND DISCUSSION

3.1 Lateral load–displacement response of single-story frames

The frames were pushed to a story drift ratio of 0.026. This value was selected because it is considered the maximum allowable story drift in TSC 2018 [2]. The Abaqus simulation demonstrated that, after yielding occurred, the frame resisted a lateral load of 271.75 kN, showing good agreement with previous research outcomes [17, 18]. In experiments of a previous study, during the hysteretic loading of frames, a bare frame resisted a peak load of 227.3 kN [17] at 86.1 mm displacement. As indicated in the previous study [18], the discrepancy between the experiments of the past study [17] and the Abaqus graph can be explained with the usage of European equivalents of Chinese materials in RC design. The frame's initial rigidity was calculated to be 14488.77 N/mm, based on the point where elasticity was first lost, corresponding to a displacement of 16.22 mm. Figure 12 illustrates the load–displacement relationship for the bare frame in the absence of any infill walls.

In SAP2000, the bare frame reached a load capacity of 257.75 kN, which was closely aligned with the result obtained from Abaqus. The calculated initial stiffness of the frame was 15103.71 N/mm, which was nearly the same as that obtained from the Abaqus analysis.

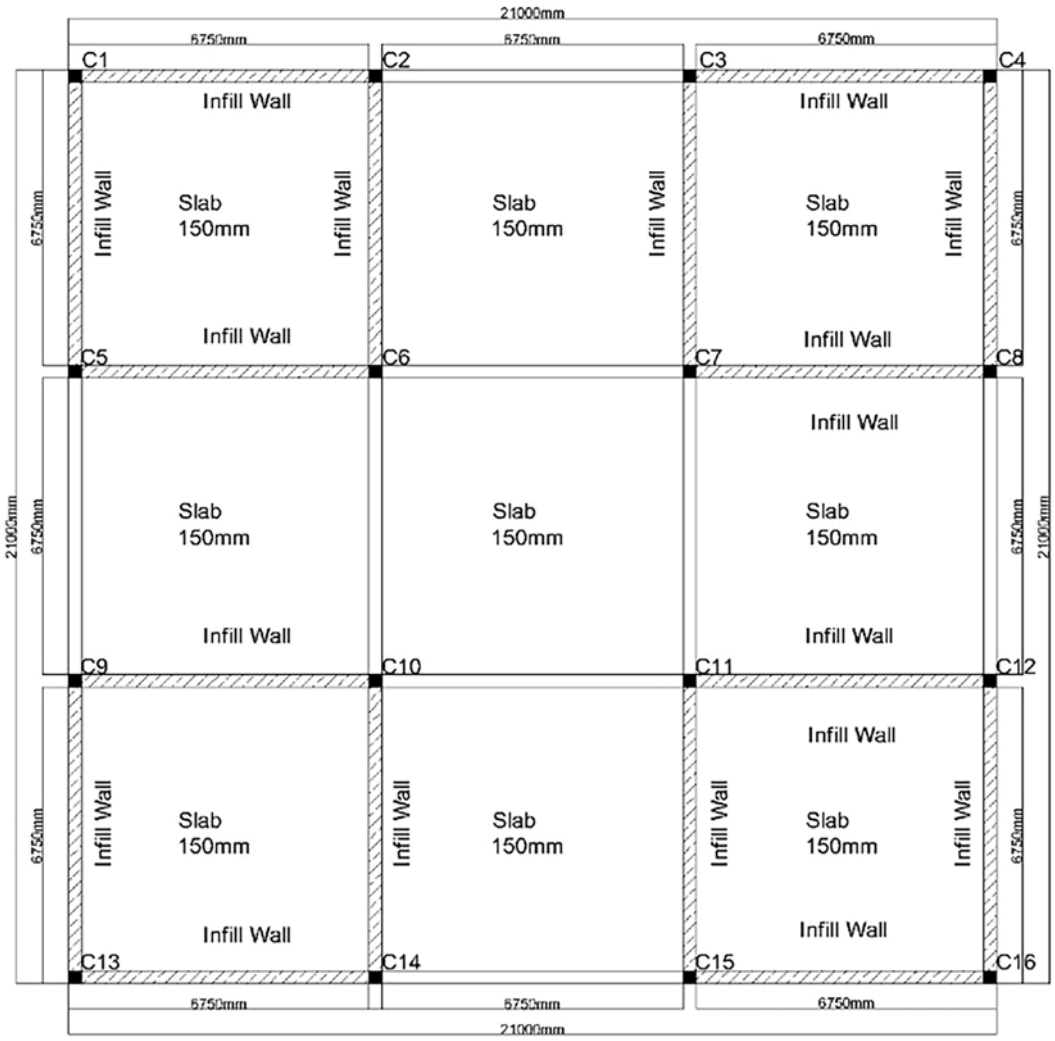

Figure 11: Plan view of the multi-story structural model developed in SAP2000.

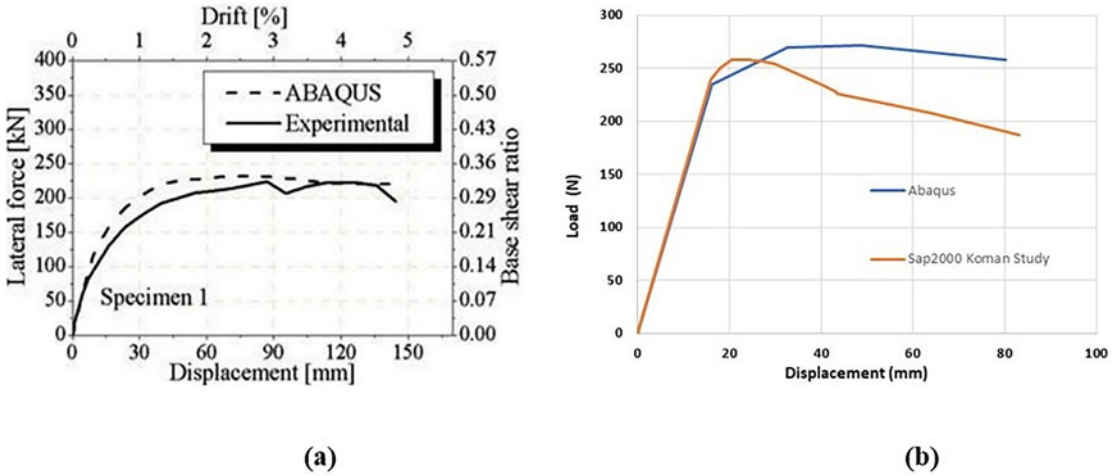

Figure 12: a) Load displacement curves of bare frame from past study [17]. b) Load displacement curves in Abaqus and in Sap2000.

Following the onset of yielding in the Abaqus simulation of the frame with hollow brick infill walls, a lateral load of 373.27 kN was carried, in agreement with earlier research [17, 18]. In a previous study [17], experiments showed that a frame with a hollow brick infill wall resisted a peak load of 332.9 kN at a displacement of 16 mm during hysteretic loading. In Abaqus analysis this result indicated a 37% increase when compared with the bare frame. Considering the displacement level of 15.72 mm, where the first loss of elasticity occurred, the initial stiffness of the frame was determined to be 19328.12 N/mm. An improvement of 33% was observed in comparison with the bare frame. In SAP2000, the load capacity was calculated as 331.41 kN, which was 11% lower than the Abaqus result. This was explained by neglecting the tensile strength of the wall in the SAP2000 analysis and modeling it as a compressive strut only. The initial rigidity in SAP2000 was calculated as 34255.89 N/mm. The frame's load–displacement response with hollow brick infill walls is shown in Figure 13.

In the Abaqus analysis, the frame with AAC blocks and polyurethane binder carried a lateral load of 460.017 kN after yielding started. This represented a 23% improvement over the frame with conventional hollow brick infill walls and a 70% enhancement relative to the bare frame. The stiffness of the frame in the elastic range was calculated as 19747.95 N/mm, based on the point corresponding to a displacement of 16.83 mm, where the first deviation from linear elastic behavior was observed. The initial rigidity was nearly the same as with a frame containing a traditional hollow brick infill wall. In the SAP2000 analysis, the frame's load capacity reached 456.87 kN, which was nearly the same as the Abaqus analysis. SAP2000 results indicated an elastic-phase stiffness of 19173.04 N/mm, which was nearly the same as the Abaqus analysis. The structural response in terms of load–displacement for the frame with AAC blocks and polyurethane binder is shown in Figure 14. The results are summarized in Table 5.

To verify the reliability of the analysis, the ratio of kinetic energy to total internal energy must be examined post-simulation, as previously discussed. Typically, maintaining the kinetic energy below 5–10% of the total internal energy is advised to ensure the accuracy of the simulation. As presented in Figure 15, the kinetic energy values for the bare frame stayed well below the corresponding strain energy levels throughout the entire loading phase. This ratio was also validated across other frame configurations, indicating that the overall analysis could be reliably classified as quasi-static. In other words, the entire frame models did not experience sufficient acceleration to be classified as dynamic loading. Therefore, the outcomes were suitable for meaningful comparison with quasi-static experimental results.

A prior study [8] employing semi-interlocking mortarless blocks to improve energy dissipation in reinforced concrete frames reported a 40% increase in lateral load capacity relative to a bare frame without infill [8]. An additional prior study reported a 33% increase in lateral load capacity with the use of an infill system featuring sliding joints [9]. The 70% increase observed in this study through the use of AAC block infill and polyurethane binders can be regarded as promising for the earthquake-resistant design of reinforced concrete structures.

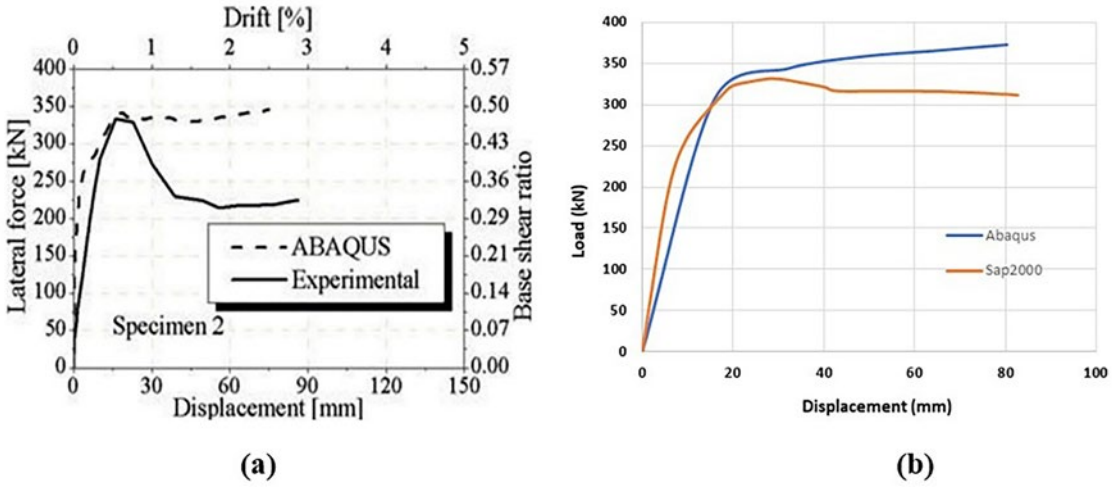

Figure 13: a) Load displacement curves of frame with hollow brick infill wall in past study [17]. b) Load displacement curves of frame with hollow brick infill in Abaqus and in Sap2000.

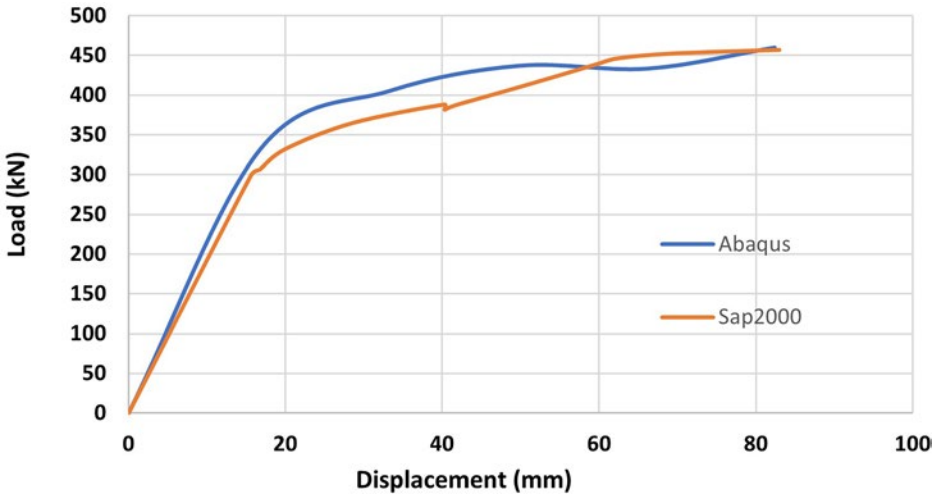

Figure 14: Load displacement graph of frame with AAC blocks and polyurethane binder.

Table 5: Comparison of results for single story frames.

	LAT. DRIFT	MAX. LAT. LOAD (EXP.) [17] (kN)	DISP. AT PEAK LOAD (EXP.) (mm)	MAX. LAT. LOAD ABAQUS (kN)	DISP. AT PEAK LOAD ABAQUS (mm)	INITIAL RIGIDITY ABAQUS (N/mm)	MAX. LAT. LOAD SAP2000 (kN)	DISP. AT PEAK LOAD SAP2000 (mm)	INITIAL RIGIDITY SAP2000 (N/mm)
Bare Frame	0.026	227.3	86.1	271.75	48.64	14488.77	257.75	24.6	15103.71
Frame with Hollow Brick Infill Wall	0.026	332.9 (46.5%)	16	373.27 (37%)	80.17	19328.12 (33%)	331.41 (28%)	29.36	34255.89 (126%)
Frame with AAC blocks and Polyurethane Binder	0.026	–	–	460.017 (70%)	82.41	19747.95 (36%)	456.87 (77%)	82.97	19173.04 (26%)

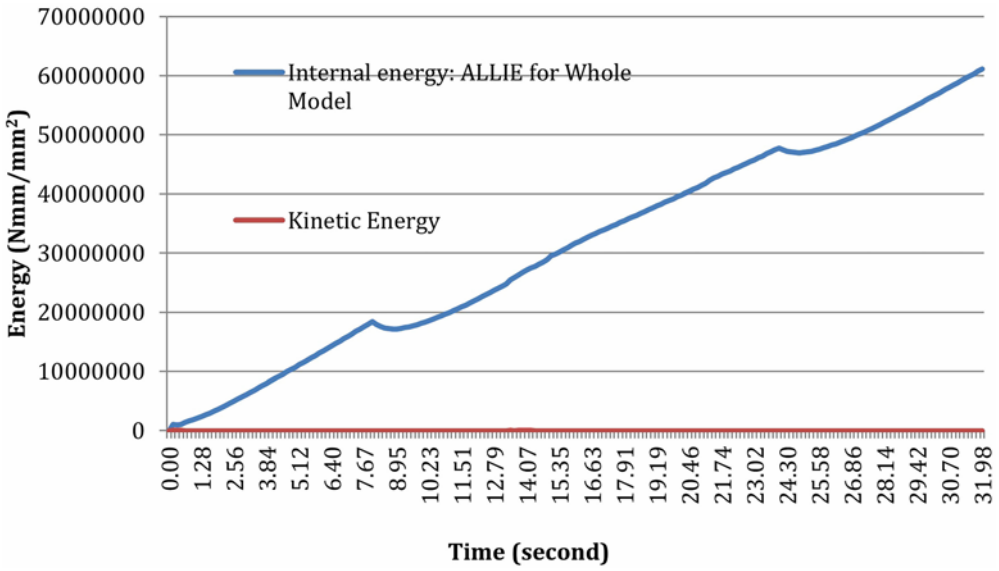

Figure 15: Internal energy for whole model vs kinetic energy comparison for bare frame.

3.2. Stresses in single story frames

In Abaqus after the analysis, it is possible to observe the Von Mises stresses in elements for different stages of loading. In a previous study [37] in which a numerical approach was performed by Abaqus to estimate the elastic properties of filler-modified asphalt binders, Von Misses stress analysis was done to identify how stresses are distributed within the glass-fiber-reinforced asphalt binder, especially around the fibers. At the maximum displacement of 80 mm, the rebars of the bare frame exhibited Von Mises stresses up to 527 MPa in the beam–column junctions. This value exceeded the steel yield strength (491 MPa) and approached its tensile strength (553 MPa). In the stirrups, the Von Mises stresses exceeded the limit of yield strength, which is 277 MPa, and reached a level around 351–395 MPa. The Von Mises stress contours for the reinforcing bars in the bare frame are shown in Figure 16. As illustrated in Figure 17, the maximum plastic strain values in the rebars varied between 0.03 and 0.058 in the beam–column junctions and at the column bases, indicating significant damage in these regions, consistent with the experimental findings of a previous study [17]. At maximum displacement level, the Von Mises stresses in the concrete of the bare frame reached around 30–35 MPa. These values exceeded the strength of the material. Figure 18 illustrates the Von Mises stresses developed in the concrete in the bare frame. Furthermore, maximum principal plastic strains varied between 0.06 and 0.1 in damaged zones, as seen in Figure 18. At a displacement level of 80 mm, the Von Mises stress in the traditional hollow brick infill wall reached 0.81 MPa in regions indicated by green shading, as seen in Figure 19. This value exceeded the tensile strength limit of 0.26 MPa of the material. Also, as seen in Figure 20, maximum principal plastic strains and equivalent plastic strains varied around 0.04 over a large portion of the wall. These values indicated damage in these zones. In the wall constructed by AAC blocks and polyurethane binder, Von Mises stresses reached

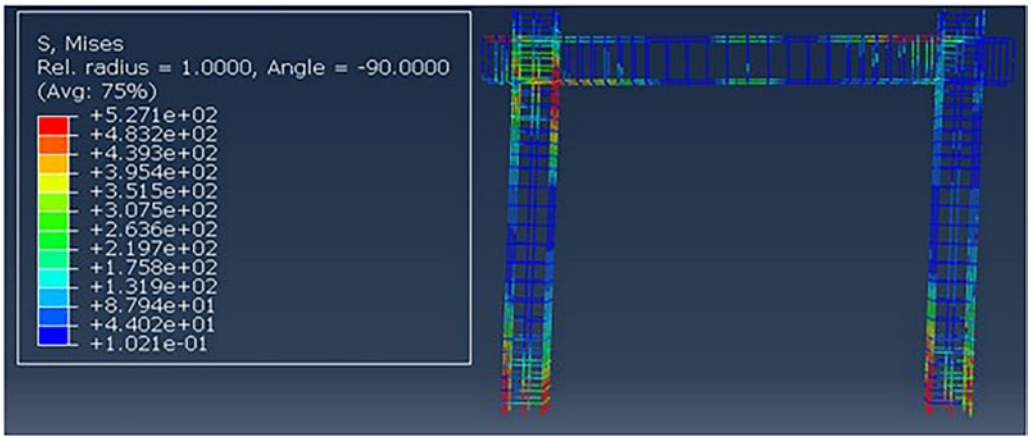

Figure 16: Von Mises stress distribution in rebars of bare frame at maximum displacement.

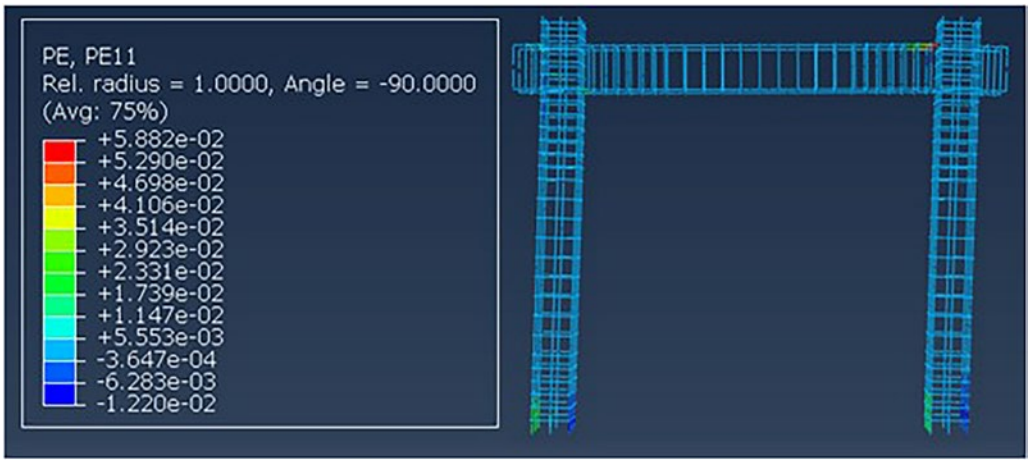

Figure 17: Plastic strains in rebars in longitudinal direction at maximum displacement of frame.

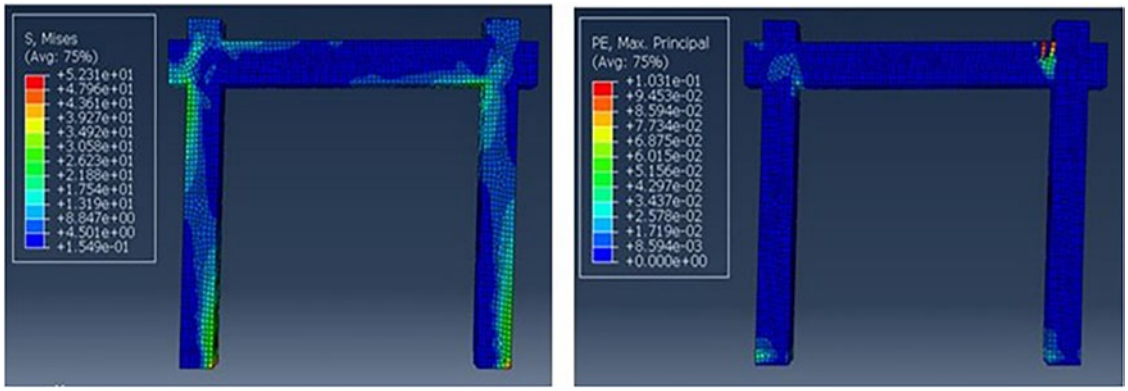

Figure 18: The Von Mises stresses in concrete of bare frame at max. displacement.

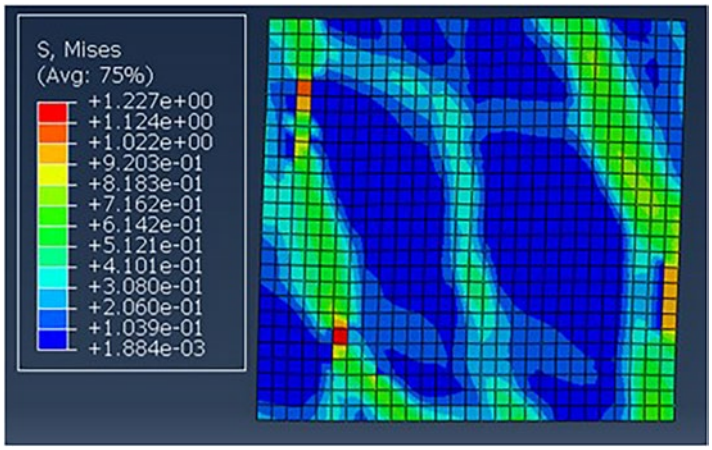

Figure 19: The Von Mises stresses in wall with traditional hollow bricks at max. displacement.

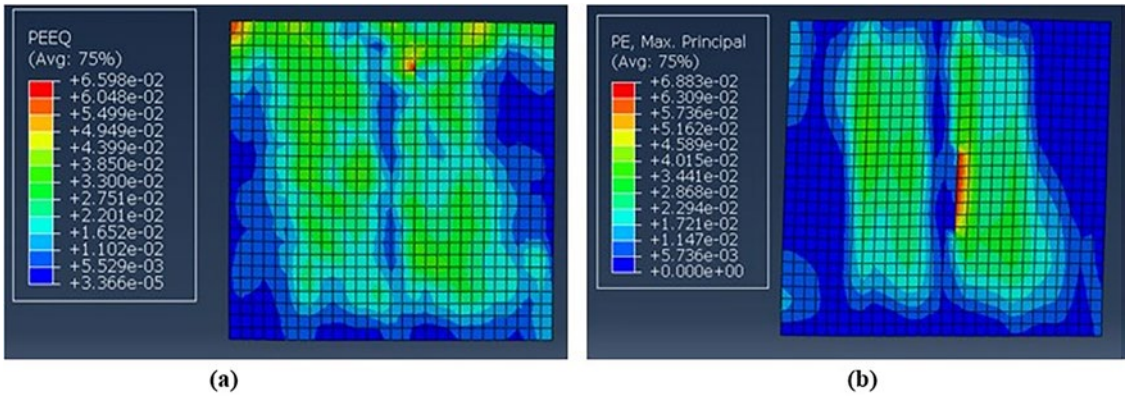

Figure 20: a) The equivalent plastic strains in traditional hollow brick wall. b) The max. principal strain in traditional infill wall at max. displacement of frame.

a level of 2.57 MPa. In AAC blocks the tensile strength is 1.44 MPa, so big damage is expected for blocks. Figure 21 displays the Von Mises stress contours observed in the AAC blocks. Figure 22 illustrates the maximum principal plastic strains and equivalent plastic strains present in the AAC block wall.

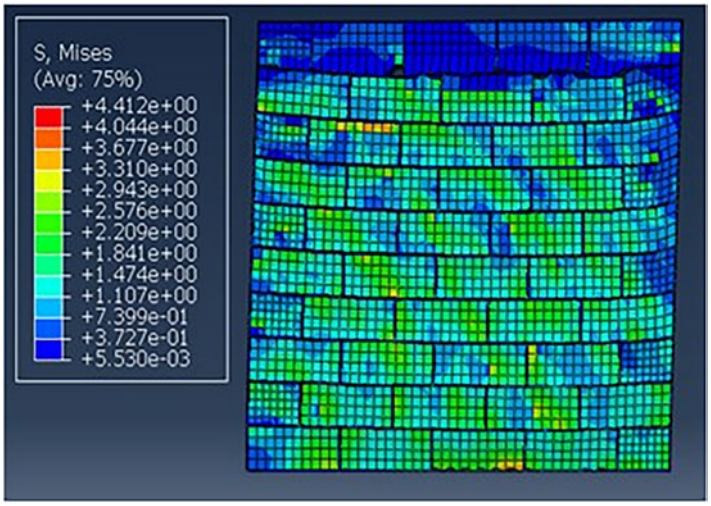

Figure 21: The Von Mises stresses in wall with AAC blocks and polyurethane binder at max. displacement.

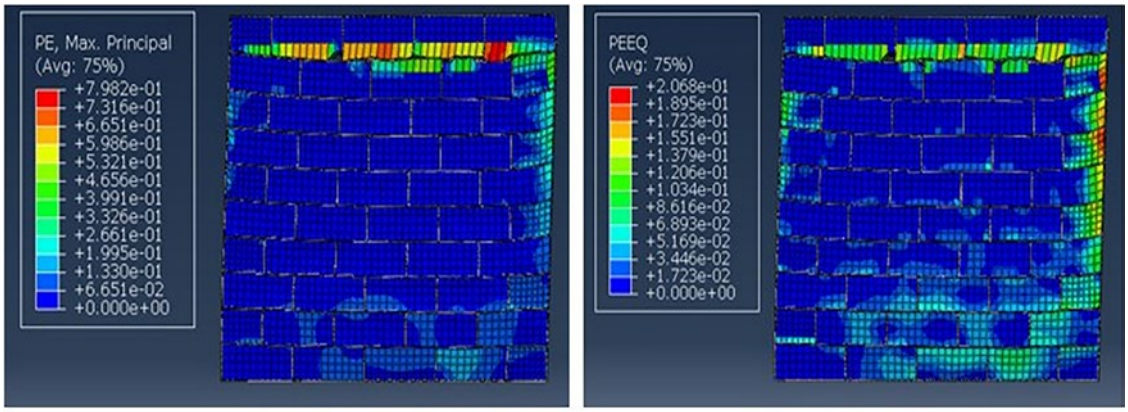

Figure 22: a) The equivalent plastic strains in AAC block wall b) The max. principal strain in AAC block wall at max. displacement of frame.

3.3. Capacity curves of multi story structures

In Figure 23, capacity curves (obtained in SAP2000) of multistory structures are shown. The capacity of the structure without any walls was detected as 3375 kN, whereas if traditional hollow brick infill walls were contained inside the structure, the capacity increased to the 3796.30 kN level (a 12% increase). The use of AAC block and polyurethane binder infill walls increased the capacity to 4667.41 kN, which was 22% higher than the structure with hollow brick infills. This level indicates an approximately 38% increase when compared with a structure without any infill. The initial stiffness of the structure without any wall can be considered as 87.32 kN/mm. The initial stiffness of the structure with hollow brick infill walls can be considered at 115.34 kN/mm (32% more than the structure without any walls). The initial stiffness of the structure with AAC blocks and polyurethane binder can be considered as 103.08 kN/mm, which was 10% smaller than the structure with traditional hollow brick infills and 18% higher than the situation without any infills. As seen in Figure 19, AAC blocks and polyurethane binder provided a more ductile behavior. If the total energy consumption (areas under pushover curves) was approximately calculated using the trapezoidal rule, it was found that the structure with AAC blocks and polyurethane binder consumed 51% more energy than the structure without any infill and 11% more energy than the structure with traditional hollow brick infill. Table 6 summarizes the results.

In FEMA-356 code, the performance level in plastic hinges was defined according to the curvature level of the hinge. Point B represents the point where yield occurs. As shown in Figure 24, FEMA-356 defines additional performance levels, namely Immediate Occupancy (IO), Life Safety (LS), and Collapse Prevention

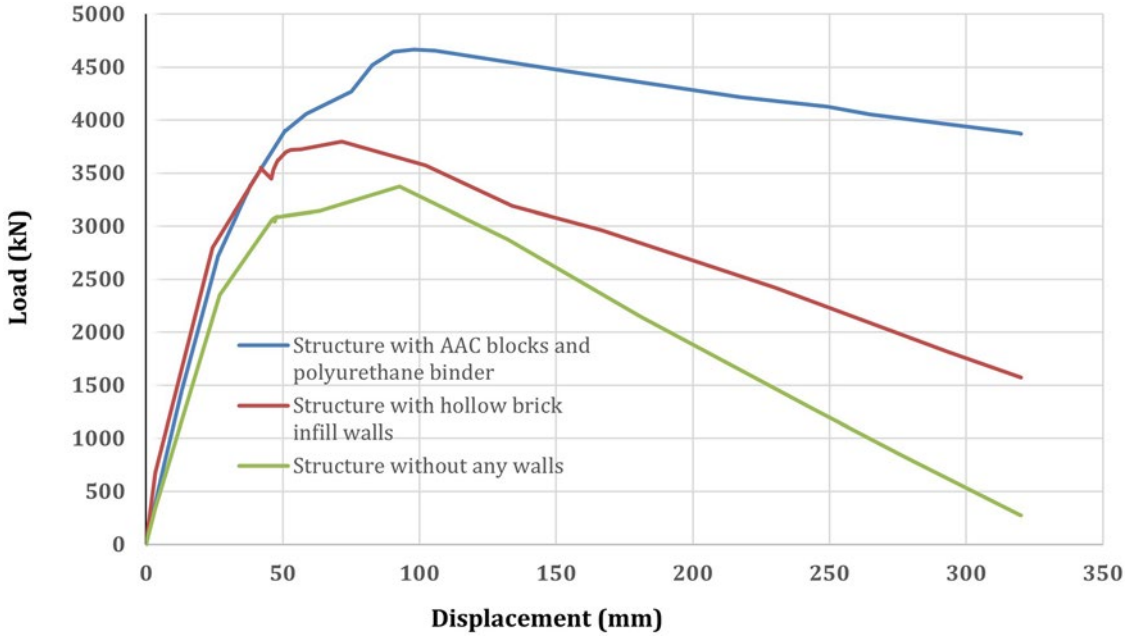

Figure 23: Capacity curves of multistory structures.

Table 6: Comparison of results for multi-story structures.

	MAX. LAT. DRIFT	MAX. LATERAL LOAD (kN)	DISP. AT PEAK LOAD SAP2000 (mm)	INITIAL RIGIDITY (SAP2000) (kN/mm)	TOTAL ENERGY CONSUMPTION (AREA UNDER PUSHOVER CURVES) (kN/mm)
Structure without any walls	0.035	3375	92.71	87.32	571521
Structure with Hollow Brick Infill	0.035	3796.30 (12%)	71.66	115.34 (32%)	802523 (40%)
Structure with AAC blocks	0.035	4667.41 (38%)	98.05	103.08 (18%)	1176684 (106%)

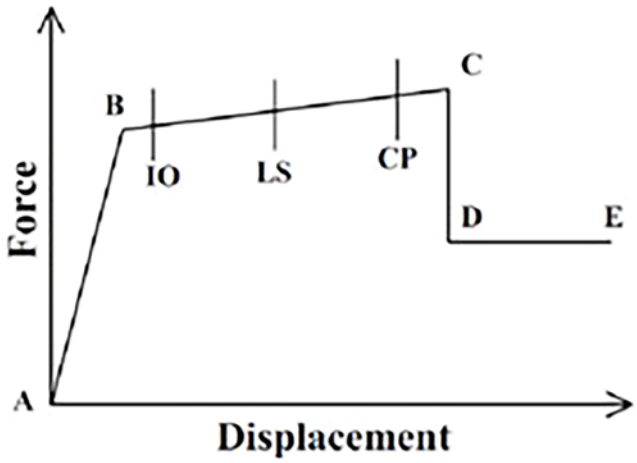

Figure 24: Plastic hinge idealization curve in FEMA-356 [38].

Table 7: Plastic hinge numbers in the last step according to the damage types.

	A TO B	B TO IO	IO TO LS	LS TO CP	CP TO C	C TO D	D TO E	BEYOND E	TOTAL
Structure without any walls	157	29	21	1	0	32	0	0	240
Structure with hollow brick infill walls	162	28	18	0	0	20	1	11	240
Structure with AAC blocks and polyurethane binder	156	23	29	0	0	32	0	0	240

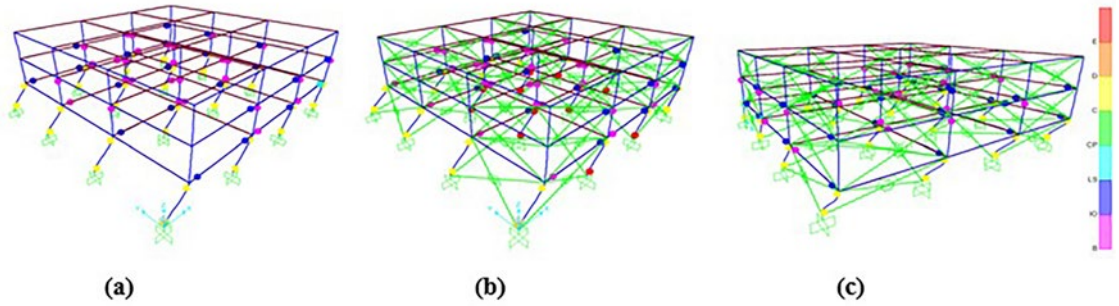

Figure 25: Performance levels of plastic hinges: a) Structure without any infill wall b) Structure with hollow brick infill c) Structure with AAC blocks and polyurethane binder.

(CP). The plastic rotation limitations for immediate occupancy (IO), life safety (LS), and collapse prevention (CP) are 0.003, 0.012, and 0.015 radians, respectively.

When the situations of plastic hinges were examined, it was seen that in the structure without any walls, 29 hinges were between the B to IO level whereas 32 hinges were between the C to D level which indicating collapse. In the structure with hollow brick walls, the performance level of 28 hinges was between B and IO damage level, 18 hinges were between IO and LS level, 0 hinges were between LS and CP level only. In the structure with AAC blocks and polyurethane binder, the performance level of 23 hinges was between B and IO damage level, 29 hinges were between IO and LS level, and no hinge was between LS and CP level. Table 7 shows the number of plastic joints in the last step according to their damage types: structure without any walls, structure with hollow brick infill walls, and structure with AAC blocks and polyurethane binder, respectively. Figure 24 depicts the distribution of plastic hinges throughout the frame. It can be observed from the plastic hinge levels that the polyurethane-infilled system exhibits higher ductility and energy dissipation capacity. Figure 25 demonstrates the situation the performance levels of hinges in the structures. In multi-story buildings subjected to lateral displacements up to 320 mm, while the traditional infilled model exceeded beyond level E, the polyurethane-infilled model was observed to remain within the C to D range. The traditional infill wall demonstrated a brittle failure mode with an abrupt stiffness degradation, which consequently resulted in more extensive damage in the plastic hinges.

4. CONCLUSIONS

A new wall system was proposed in this study to enhance the performance of RC moment-resisting frame structures. The wall system consisted of AAC blocks and polyurethane binder. In the study a 250 mm thick AAC block with 5 MPa compressive strength was used. First, a validation was done in single-story frames using both Abaqus and SAP2000 softwares, and the results of the bare frame and the results of the frame with hollow brick infill were compared with previous experimental and numerical studies [17, 18]. The results showed a good level of consistency. The analysis in single-story frames indicated that the proposed infill provides a bigger lateral

load capacity than traditional hollow brick infills, and post-peak behavior is better than bare frame. The proposed infill exhibited larger displacement at peak load than the hollow brick infill, indicating better deformation capacity before failure. In this study, based on the Abaqus analyses, the proposed infill wall increased the initial stiffness of the RC frame to a similar extent as a conventional hollow brick wall. Considering that, in construction practice, infill walls are also built using mortar and bricks with higher strength, it would be more reasonable and likely to use the proposed infill wall not primarily as an element to increase lateral stiffness, but rather as a structural component that enhances ductility and energy dissipation. Modelling the infills using link elements in SAP2000 software showed good agreement with Abaqus analysis.

The stress and strain analysis in single-story frames showed that in max. drift ratio, high damage must be expected in both of the infill walls. Future studies can utilize blocks with higher strength to improve the overall performance of the RC frame. Subsequently, the modeling approach using link elements in SAP2000 software was applied to 3-story RC moment frame structures to represent the behavior of infill walls. The results indicated that the proposed infill system increased the lateral load-carrying capacity and energy dissipation when compared with structures containing traditional infill walls and no infill walls. While hollow brick infill slightly reduced peak displacement, AAC block infill maintained a relatively large displacement capacity, suggesting improved ductility in addition to higher strength. Usage of proposed infill walls decreased the damage in plastic hinges. The highly deformable polyurethane binder is expected to help the wall to prevent segregation of blocks.

In the following studies, it's advised to investigate the proposed system experimentally and numerically. As a conclusion, AAC block and polyurethane binder wall are high prospects for the future to be used in the design of RC structures in earthquake-proof zones.

5. ACKNOWLEDGMENTS

No support was taken during the preparation of article.

6. BIBLIOGRAPHY

[1] KARAKALE, V., ÖZGÜR, E., ATAOĞLU, Ş., "Site observations on buildings' performance in hatay province after Kahramanmaraş earthquakes", *El-Cezerî Journal of Science and Engineering*, v. 10, n. 2, pp. 506–516, 2023. doi: https://doi.org/10.31202/ecjse.1253284.

[2] TÜRKIYE, Turkish Seısmıc Code, *Specifications for buildings to be built in seismic areas*, Ankara, Ministry of Public Works and Settlement, 2018.

[3] ÇALIM, F., GÜLLÜ, A., YÜKSEL, E., "Comparison of various input energy spectra for the february 6th 2023 Kahramanmaraş earthquake sequence", *Journal of Earthquake Engineering*, v. 1, n. 20, pp. 1–20, May 2024. doi: https://doi.org/10.1080/13632469.2024.2336202.

[4] LI, H., LI, G., WANG, S. "Study and Application of Metallic Yielding Energy Dissipation Devices in Buildings", In: *10th National Conference on Earthquake Engineering*, Alaska, USA, 21–25 July 2014. doi: https://doi.org/10.4231/D3FQ9Q593.

[5] MULLETI, E., *Seismic response of high-rise buildings using friction dampers*, Tiranë, Albania, Epoka University, 2014.

[6] AMATO, G., FOSSETTI, M., CAVALERI, L., *et al.*, "An updated model of equivalent diagonal strut for infill panels", In: Cosenza, E. (ed), *Eurocode 8 perspectives from the Italian Standpoint*, Napoli, Italy, Doppiavoce, pp. 119–128, 2009.

[7] TOTOEV, Y.Z., LIN, K., "Frictional energy dissipation and damping capacity of framed semi interlocking masonry infill", In: *15th International Brick and Block Masonry Conference*, Florianopolis, Brazil, 3–6 June 2012.

[8] SANADA, Y., YAMAUCHI, N., TAKAHASHI, *et al*., "Interlocking block infill capable of resisting out-of-plane loads", In: *The 14th World Conference on Earthquake Engineering*, Beijing, 12–17 October 2008.

[9] MILANESI, R.R., TOTOEV, Y., MORANDI, *et al.*, "Estimation of basic dynamic characteristics of pliable masonry infills with horizontal sliding joints from in plane test results", In: *7th Eccomas Thematic Conference on Computational Methods in Structural Dynamics and Earthquake Engineering*, Crete, Greece, pp. 2543–2564, 24–26 June 2019. doi: doi: https://doi.org/10.7712/120119.7093.19097.

[10] HOSSAIN, A., TOTOEV, Y., MASIA, M.J. "Energy dissipation of framed semi interlocking masonry panel under large displacement", In: *10th Australian Masonry Conference*, Sydney, Australia, pp. 344–355, 11–14 February 2018.

[11] GUPTA, A., MEENA, G., SINGHAL, V.K, "Strengthening of autoclaved aerated concrete (AAC) masonry wallettes with fabric reinforced cementitious matrix for in-plane shear and out-of-plane loads", *Structures*, v. 51, pp. 1869–1880, 2023. doi: https://doi.org/10.1016/j.istruc.2023.03.099.

[12] GUPTA, A., SINGHAL, V., "Strengthening of confined masonry walls using reinforced cementitious matrix subjected to in-plane loads:a state-of-the-art review", *Journal of Earthquake Engineering*, v. 28, n. 5, pp. 1404–1420, 2024. doi: https://doi.org/10.1080/13632469.2023.2233029.

[13] MEMON, K.K., GUPTA, A., GOUR, C.P., "Structural performance of externally bonded composite systems for masonry wall strengthening", *Australian Journal of Structural Engineering*, pp. 1–10, 2025. doi: https://doi.org/10.1080/13287982.2025.2476273.

[14] GUPTA, A., SINGHAL, V., "Strengthening of confined masonry walls with openings using externally bonded reinforced composites", *Journal of Composites for Construction*, v. 29, n. 4, pp. 402–503, 2025. doi: https://doi.org/10.1061/JCCOF2.CCENG-5042.

[15] AKYILDIZ, A.T., KWIECIEN, A., ZAJAC, B., *et al.*, "Preliminary in plane shear tests of infills protected by PUFJ interfaces", In: Kubica, J., Kwiecień, A., Bednarz, L. (eds), *Brick and block masonry - From historical to sustainable masonry*, London, CRC Press, pp. 968–975, 2020. doi: https://doi.org/10.1201/9781003098508-137.

[16] ROUSAKIS, T., PAPADOULI, E., SAPALIDIS, *et al.*, "Flexible Joints between RC frames and masonry infill for improved seismic performance – shake table tests", In: Kubica, J., Kwiecień, A., Bednarz, L. (eds), *Brick and block masonry – From historical to sustainable masonry*, London, CRC Press, pp. 499–507, 2020. doi: doi: https://doi.org/10.1201/9781003098508-68.

[17] ZHAI, C., KONG, J., WANG, X., *et al.*, "Experimental and finite element analytical investigation of seismic behavior of full-scale masonry infilled RC frames", *Journal of Earthquake Engineering*, v. 20, n. 7, pp. 1171–1198, 2016. doi: https://doi.org/10.1080/13632469.2016.1138171.

[18] KOMAN, H., "A proposal for strengthening of RC structures by using high strength lightweight concrete panels and polyurethane binders", *Erciyes University Journal of the Institute of Science and Technology*, v. 39, n. 3, pp. 521–537, 2023.

[19] SANTOS, C.F.R., ALVARENGA, R.C.S.S., RIBERIO, J.C.L., *et al.* "Numerical and Experimental Evaluation of Masonry Prisms By Finite Element Method", *Ibracon Structure and Materials Journal*, v. 10, n. 2, pp. 477–508, 2017. doi: https://doi.org/10.1590/S1983-41952017000200010.

[20] OBAIDAT, Y.T., "*Structural retrofitting of concrete beams using FRP*", D.Sc. Thesis, Lund University, Lund, 2011.

[21] INCULET, V., ANDERSEN, L.V., "Nonlinear analysis of earthquake induced vibrations", M.Sc. Thesis, Aalborg University School of Engineering and Science, Aalborg, Denmark, 2016.

[22] JAKEL, R., "Analysis of hyperelastic materials with mechanica - theory and application examples", In: 2nd SAXSIM, Chemnitz, 27 April 2010.

[23] KWIECIEN, A., "Shear bond of composites to brick applied highly deformable in relation to resin epoxy interface materials", *Materials and Structures*, v. 47, n. 12, pp. 2005–2020, 2014. doi: https://doi.org/10.1617/s11527-014-0363-y.

[24] KWIECIEN, A., "Highly deformable polymers for repair and strengthening of cracked masonry structures", *GSTF Journal of Engineering Technology*, v. 2, n. 1, pp. 182–196, 2013. doi: https://doi.org/10.5176/2251-3701_2.1.53.

[25] KSIEL, P., "*Model approach for polymer flexible joints in precast elements joints for concrete pavements*", M.Sc. Thesis, Krakow University of Technology, Krakow, Poland, 2018.

[26] GUPTA, A., SINGH, A.K., SINGHAL, V., *et al.*, "Numerical simulation of interaction properties at wall-to-tie-column interface for confined masonry walls", *Construction & Building Materials*, v. 411, pp. 134139, 2024. doi: https://doi.org/10.1016/j.conbuildmat.2023.134139.

[27] ABDULLA, K.F., CUNNINGHAM, L.S., GILLIE, M., "Simulating masonry behavior using a simplified micro model approach", *Engineering Structures*, v. 151, pp. 349–365, 2017. doi: https://doi.org/10.1016/j.engstruct.2017.08.021.

[28] KOMAN, H., NOHUTCU, H., KILIÇ, G., *et al.*, "Improving the seismic behaviour of RC frames with mortarless blocks", *Građevinar*, v. 77, n. 3, pp. 219–236, 2025. doi: https://doi.org/10.14256/JCE.3920.2023.

[29] VISKOVIC, A., ZUCCARINO, L., KWIECIEN, A., *et al.*, "Quick seismic protection of weak masonry infilling in filled frame structures using flexible joints", *Key Engineering Materials*, v. 747, pp. 628–637, 2017. doi: https://doi.org/10.4028/www.scientific.net/KEM.747.628.

[30] ÖZEREN, Ö., "*Donatılı Gazbeton Paneller ve Bu Paneller ile Yapılan Binaların Düşey ve Yatay Yükler Altında Davranışı*", M.Sc. Thesis, Istanbul Technical University, Istanbul, Türkiye, 2016.

[31] KOMAN, H. "*Improving the earthquake behavior of structures by using mortarless blocks*", Manisa Celal Bayar University, Manisa, Türkiye, 2021.

[32] GUPTA, A., SINGHAL, V. "Parametric finite element analysis of confined masonry walls strengthened with fabric reinforced cementitious matrix", In: Shrikhande, M., Agarwal, P., Kumar, P.C.A. (eds), *Proceedings of 17th Symposium on Earthquake Engineering*, Singapore, Springer, v. 2, pp. 111–123, 2023. doi: https://doi.org/10.1007/978-981-99-1604-7_9.

[33] DEMIR, C., "*Seismic Behavior of Historical stone masonry*", Istanbul Technical University, Istanbul, Türkiye, 2012.

[34] CAVALERI, L., DI TRAPANI, F., "Cyclic response of masonry infilled RC frames: experimental results and simplified modeling", *Soil Dynamics and Earthquake Engineering*, v. 65, pp. 224–242, 2014. doi: https://doi.org/10.1016/j.soildyn.2014.06.016.

[35] MAHMUD, E., BONEV, Z., ABDULAHAD, E., "Nonlinear seismic analysis of masonry infilled RC frame structures", *Građevinski Materijali i Konstrukcije*, v. 62, n. 1, pp. 17–25, 2019. doi: https://doi.org/10.5937/GRMK1901017M.

[36] KÖMÜRCÜ, S., "*Yığma Duvarların Düzlemiçi Davranışlarının Modellenmesi ve Analizi*", M.Sc. Thesis, Istanbul Technical University, Istanbul, Türkiye, 2017.

[37] ZHANG, S., KIRUMIRA, N., "Numerical prediction of elastic properties of filler-modified asphalt binders using finite element analysis", *Matéria*, v. 30, pp. e20250156, 2025. doi: https://doi.org/10.1590/1517-7076-rmat-2025-0156.

[38] COMPUTERS AND STRUCTURES INC., *SAP2000, Integrated Software for Structural Analysis and Design*, Berkeley, California, Computers and Structures Inc.